Published in final edited form as:
Nature. ; 479(7372): 203–207. doi:10.1038/nature10569.

Two types of photoluminescence blinking revealed by single quantum dot spectroelectrochemistry

Christophe Galland[1,2], **Yagnaseni Ghosh**[3], **Andrea Steinbrück**[3], **Milan Sykora**[1,*], **Jennifer A. Hollingsworth**[3], **Victor I. Klimov**[1,2,*], and **Han Htoon**[1,3,*]

[1]Chemistry Division, Los Alamos National Laboratory, Los Alamos, NM 87545, USA

[2]Center for Advanced Solar Photophysics, Los Alamos National Laboratory, Los Alamos, NM 87545, USA

[3]Materials Physics & Applications Division: Center for Integrated Nanotechnologies, Los Alamos National Laboratory, Los Alamos, NM 87545, USA

Abstract

Photoluminescence (PL) intermittency (blinking), or random switching between states of high- (ON) and low (OFF) emissivities, is a universal property of molecular emitters exhibited by dyes[1], polymers[2], biological molecules[3] and artificial nanostructures such as nanocrystal quantum dots, carbon nanotubes, and nanowires[4,5,6]. For the past fifteen years, colloidal nanocrystals have been used as a model system for studies of this phenomenon.[5,6] The occurrence of OFF periods in nanocrystal emission has been commonly attributed to the presence of an additional charge[7], which leads to PL quenching by nonradiative Auger recombination.[8] However, the "charging" model was recently challenged in several reports.[9,10] Here, to clarify the role of charging in PL intermittency, we perform time-resolved PL studies of individual nanocrystals while controlling electrochemically the degree of their charging. We find that two distinct mechanisms can lead to PL intermittency. We identify conventional blinking (A-type) due to charging/discharging of the nanocrystal core when lower PL intensities correlate with shorter PL lifetimes. Importantly, we observe a different blinking (B-type), when large changes in the PL intensity are *not* accompanied by significant changes in PL dynamics. We attribute this blinking behavior to charge fluctuations in the electron-accepting surface sites. When unoccupied, these sites intercept *hot* electrons before they relax into emitting core states. Both blinking mechanisms can be controlled electrochemically and under appropriate potential blinking can be completely suppressed.

In the conventional blinking model (Fig. 1a), ON and OFF periods correspond to a neutral and a charged nanocrystal, respectively, while photo-assisted charging/discharging causes random switching between these two states. The dynamics of the bright state is dominated by radiative recombination of the neutral exciton, X^0 (Fig. 1b), which is characterized by a long, mono-exponential decay (15 – 30 ns in CdSe nanocrystals[15–17]). For a charged exciton (trion), X^-, three-particle Auger recombination opens a fast nonradiative channel, resulting in a shorter lifetime (few nanoseconds or less), and consequently, a reduced PL quantum yield (QY). As illustrated in Figs. 1c and 1d, this model predicts correlated fluctuations of the PL intensity and the PL lifetime (referred to here as A-type blinking) that have indeed been observed experimentally[15,16,18]. Photocharging can lead to "binary" switching between the ON and the OFF states (Fig. 1c) when the time-scale of charge fluctuations is longer than the experimental binning time (typically at least tens of milliseconds). As we discuss below, the same discrete charging process can also produce quasi-continuous PL

*To whom correspondence should be addressed: klimov@lanl.gov (V.I.K); htoon@lanl.gov (H.H.); sykoram@lanl.gov (M.S.).

fluctuations, referred to as "flickering" (Fig. 1d). In this case, the data within each bin represents an average over the neutral and charged nanocrystal states, which results in PL intensities and lifetimes that vary continuously according to the relative times spent by the nanocrystal in each charge state.

A convenient tool for the analysis of correlations between PL intensities and lifetimes is a Fluorescence Lifetime – Intensity Distribution (FLID) representation. In this representation, the probability to occupy a given state in the two-dimensional "PL intensity – lifetime" space is shown by false color, which changes from blue to red with increasing number of occurrences. As illustrated in the insets of Figs. 1c and 1d, the use of FLIDs allows one to readily identify different types of charge states as well as different types of blinking behaviors (e.g., binary blinking versus flickering).

In our work, to verify the validity of the charging model of PL intermittency, we combine single-nanocrystal spectroscopy with an electrochemical approach for controlling the extent of nanocrystal charging[19,20,21]. Specifically, we conduct single-nanocrystal, time-tagged, time-resolved, single-photon counting studies of samples incorporated into a 3-electrode electrochemical cell (Fig. 2a). We investigate core/shell CdSe/CdS nanocrystals synthesized according to Ref. 11. In the case of exceptionally thick, 16 – 19 monolayer (ML) shells, they exhibit nearly complete suppression of blinking.[11] Here, we use nanocrystals with intermediate shell thicknesses (7 – 9 MLs) that show typical blinking behaviors, but with a QY during OFF periods which is considerably higher compared to that in standard nanocrystals. This allows us to investigate in detail the properties of the OFF state, and the effect of controlled charging on its emissivity and dynamics. All changes in PL intensity and dynamics induced by the applied potential are reversible, indicating no permanent chemical or photochemical modifications of the nanocrystals and suggesting that these changes are due to controlled charging/discharging. To verify that the observed PL originates from a single nanocrystal, we measure the second-order intensity correlation function[14], g_2, and ensure that $g_2(0) < 0.5$ (inset in Fig. 2b). All experiments are performed under ambient conditions at room temperature. All potentials are reported with respect to a silver wire quasi-reference (see Methods for further experimental details).

Figure 2b presents PL dynamics for a single nanocrystal under increasing negative potential (V), which corresponds to electron injection. The PL decay becomes progressively faster for more negative V. All decays can be fitted globally to a three-exponential function shown by grey lines in Fig 2b. The high fidelity of the fit (see residuals in the inset) suggests that only three distinct emitting states are involved, each having a well-defined PL lifetime: $\tau^s = 2$ ns, $\tau^m = 5$ ns and $\tau^l = 24$ ns. As V is increased from 0 to −0.7 V, the weight of the τ^m component gradually increases relative to the τ^l component. At more negative V, the fastest τ^s component emerges and becomes dominant at −1.1 V. We assign these three lifetimes to three distinct states: neutral (τ^l), singly (τ^m), and doubly (τ^s) charged excitons. Due to increased rates of radiative decay, singly charged excitons (negative trions) show increased signal at short times compared to neutral excitons (Figs. 2b); however, the time-integrated PL signal is reduced because of Auger recombination. The observed shortening of PL decay upon charging is due to enhancement in both the radiative and nonradiative decay rates.

To confirm the above assignments and investigate the relationship between charging and blinking, we analyze the correlations in the temporal variations of PL decay time and PL intensity. In Fig. 3, we plot PL intensity and average lifetime trajectories (calculated for a 50 ms bin size; see Supplementary Information) along with corresponding FLIDs for the nanocrystal shown in Fig. 2. To illustrate the variability in blinking behaviors, in panels (a) and (b), we present the data collected for this nanocrystal on two different days. These data, representing examples of binary ON/OFF switching (a) and flickering (b), indicate a strong

correlation between the PL intensity and the PL lifetime during the fluctuations, in agreement with the conventional charging model. We denote this behavior as A-type blinking.

In Fig 3a, at 0 V (middle panel), the nanocrystal displays binary blinking between the neutral (X^0) and the singly charged (X^-) state. The average PL lifetime of X^0 (ON state) is τ^l ~24 ns and corresponds to a radiative lifetime of ~60 ns (see Supplementary Information), which is in agreement with previous ensemble studies of this type of nanocrystals.[17] Application of a positive $V = +0.6$ V (left panel) dramatically suppresses charge fluctuations and results in almost nonblinking emission from the neutral exciton (see corresponding FLID and Supplementary Figs. 1 and 2; another example is shown in Supplementary Fig. 12). At a negative $V = -0.6$ V, the peak of the PL distribution shifts to the lower emissivity X^- state characterized by the ~5 ns lifetime (right in Fig. 3a). Assuming a "statistical" scaling of recombination rates with the number of charges (see Supplementary Information and Ref. 22), we deduce the Auger lifetime for X^- of ~3.5 ns. This is much shorter than the radiative lifetime of X^- (~30 ns), which explains the relatively low PL QY of the negative trion. The existence of fluctuations between X^0 and Xis indicated by a well-resolved trace in the FLID connecting the two states. We simulate the FLID data assuming that the PL intensity during a given time bin is determined by the relative times spent by the nanocrystal in the X^- and the X^0 states (see Supplementary Information). A very good agreement, without any adjustable parameters, between the simulated trace (white line) and the measured FLID provides strong support for both the assignment of emitting states and the model used in the analysis.

Interestingly, the same nanocrystal measured on a different day (Fig. 3b) shows a more continuous distribution of PL intensities and lifetimes, typically referred to as flickering. This change in the blinking behavior likely occurs as a result of shortening of time spent by the nanocrystal in a given charge state, which leads to fast switching between X^0 and X^- within the bin time used in the measurements. PL from X^- becomes dominant at $V = -0.7$ V (FLID in the middle of Fig. 3b). By applying a more negative $V = -1.1$ V, we detect a new state with lifetime τ^s ~2 ns, associated with the formation of a doubly charged exciton X^{2-} with the Auger lifetime of ~1.2 ns. Based on the FLID (Fig. 3b; right), fluctuations still occur between the X^{2-} and the X^- states.

Figure 4a presents the data from a different nanocrystal, which exhibits an unusual blinking behavior that we refer to as B-type blinking. Specifically, at $V = 0$ V (Supplementary Fig. 3) and $V = +0.8$ V (Fig. 4a; left), we observe periods of low PL intensity that are *not* accompanied by significant shortening of PL lifetimes. In fact, the PL time constant measured for the B-type OFF state is identical to that of the ON (X^0) state. These B-type blinking events were observed in 20 of the 23 dots we studied (Supplementary Table 1) and they usually coexisted with A-type fluctuations (Supplementary Fig. 3). Importantly, at $V = -1$ V, we achieve a complete suppression of blinking while preserving a long PL lifetime (~26 ns) typical of a neutral exciton. This suppression could be achieved in the majority of the nanocrystals with the B-type blinking, however, the potential required to obtain the suppression varied widely from dot to dot (from −0.6 V to −1.4 V, see Supplementary Table 1). For some nanocrystals, the elimination of B-type blinking occurred simultaneously with the onset of A-type fluctuations between X^0 and X^- (see below). At a more negative potential ($V = -1.2$ V in Fig. 4a), we observe clear signatures of electron injection into the nanocrystal. The PL decay becomes bi-exponential with increasing contribution from the negative trion with ~6 ns lifetime (see Supplementary Fig. 4). In this case, switching between X^0 and X^- occurs much faster than the bin time, which gives rise to a narrow PL intensity – lifetime distribution. As with the data in Fig. 3, we can closely reproduce this pattern using the charging model (simulated white lines in FLID).

To explain B-type blinking, we invoke the activation/deactivation of nonradiative recombination centers "*R*" that efficiently capture *hot* electrons before they relax into the lowest energy emitting state (Fig. 4b). Such processes of hot-electron trapping have been recently observed for both nanocrystals in solutions[23] and surface dispersed particles.[24,25] In this scenario, PL dynamics during the OFF periods should be similar to those of a neutral exciton while the emission intensity will be reduced according to the ratio between the rates of intraband relaxation (γ_B) and hot-electron capture by the recombination center (γ_D). Since the frequency of B-type blinking events is controlled by the electrochemical potential, the activation/deactivation of the by-pass channel is likely associated with emptying/filling of the corresponding surface trap state. Under positive potential ($V = +0.8$ V in Fig. 4a), the Fermi level shifts down in energy, which increases the relative time spent by the trap in the unoccupied (i.e., active) state and leads to increased occurrence of B-type OFF events (Fig. 4b; left). The trapped electron can recombine nonradiatively with a valence-band hole before the next photoexcitation, event leaving behind a neutral dot. Occasionally, photon absorption occurs before re-neutralization of the dot, which results in a *positive* trion (X^+); Auger decay of X^+ could explain observations of shorter PL lifetimes within the B-type OFF periods illustrated in Supplementary Fig. 5.

For a negative potential, the Fermi level shifts upward, and eventually a regime is reached where the trap states become populated and $\gamma_D \rightarrow 0$ due to Coulomb blockade ($V = -1$ V in Figs 4a and 4b). In this case, B-type blinking is completely suppressed. Application of a more negative potential eventually leads to charging of the nanocrystal core with an extra electron and emission from negative trions ($V = -1.2$ V in Figs 4a and 4b).

Blinking suppression due to filling of electron-accepting trap sites is consistent with previous observations that electron-donating thiolates enhance ensemble PL emission[26] and reduce blinking.[27] Similar phenomena were observed for other electron-donating molecules[28] as well as *n*-doped substrates.[29] Additionally, recent ultrafast studies of carrier surface trapping in ensembles of CdSe nanocrystals suggest direct relevance of this process to the problem of nanocrystal blinking[30]. These literature observations of a significant effect of surface species on PL intermittency imply that the trap sites responsible for B-type blinking are likely of surface origin.

The distinct nature of processes responsible for A- and B-type blinking is evident from the effect of increasing shell thickness on PL intermittency. Specifically, we observe that as the outer shell gets thicker, the B-type type blinking events become less frequent until they are *completely* eliminated for shells with 15 or more CdS MLs. On the other hand, the A-type blinking can still be observed even in the case of the ultra-thick 19 ML shells. The analysis of PL intermittency in more than twenty 15 ML shell nanocrystals (see Supplementary Table 2 and Supplementary Figs. 7 – 8) indicates that ~70% of these dots are nonblinking while the rest shows the A-type blinking behavior; none of the nanocrystals showed any detectable B-type blinking. In contrast, B-type blinking is clearly the dominant behavior in 7 – 9 ML shell nanocrystals (Supplementary Table 1). The fact that B-type blinking gets quickly suppressed with increasing shell thickness is consistent with the proposed mechanism of hot-electron tunneling outside the nanocrystal as this process is expected to be extremely sensitive (exponentially) to the thickness of the tunneling barrier.

The studies of statistics of ON and OFF times also indicate a clear distinction between the A-and B-type blinking mechanisms. In Fig. 5a, we show a nanocrystal displaying B-type blinking at −0.8 V, which switches to A-type blinking at −1 V. Remarkably, whereas the B-type ON and OFF times both follow a power-law distribution over almost 3 decades, the distributions of ON/OFF times in the A-type blinking regime are quasi-exponential with a cut-off time of ~70 ms (Fig. 5b). This electrochemically controlled switching between

different blinking statistics in the *same* nanocrystal is another strong indication that the difference between A- and B-type blinking is linked to the distinct nature of the underlying physical mechanisms but *not* to dot-to-dot variations. Further, the fact that the cut off time measured in the case of A-type blinking is close to a typical bin size used in the measurements suggests that relatively small changes in the time scale of charge fluctuations can result in switching between binary blinking and flickering as seen, for example, in Fig. 3.

To summarize, our studies of single-nanocrystal PL under controlled charge injection reveal two distinct types of blinking events (A and B). For A-type blinking, the changes in PL intensity correlate with changes in PL lifetime and are due to charge fluctuations in the nanocrystal core. During B-type blinking events, low-emissivity periods occur *without* significant shortening of the PL lifetime. This behavior can also be explained by charge fluctuations, however, not in the nanocrystal core but in some surface sites. When unoccupied, these sites act as efficient hot-electron traps that intercept the photoexcited hot electron before it relaxes into the emitting core state. Using an appropriate potential, we can close this channel (by filling the traps) and achieve a complete suppression of blinking.

Methods

Materials

Cadmium oxide, oleic acid (90%), 1-octadecene (ODE, 90%), 1-octadecane (OD, 90%), oleylamine, sulfur, selenium pellet, and trioctylphosphine (TOP) were purchased from Aldrich and used without further purification. Trioctylphosphine oxide (TOPO) (90%) was purchased from Strem and used without further purification.

Nanocrystal synthesis

A 100 ml round bottom (r.b.) flask equipped with a reflux condenser and a thermocouple probe was charged with 1 g of TOPO, 8 ml of ODE and 0.38 mmols of Cd-oleate under standard air-free conditions. The reaction system was evacuated for 30 minutes at room temperature and 30 minutes at 80 °C, and then the temperature was raised to 300 °C under Argon, following which a mixture of 4 mmol of TOP-Se, 3 ml oleylamine and 1 ml of ODE was quickly injected into the reaction system. The temperature was then lowered to 270 °C for CdSe nanocrystal growth. After several minutes, the solution was cooled down to room temperature, and CdSe nanocrystals (diameter, $d = 3$ nm) were collected by precipitation with ethanol and centrifugation. The CdSe nanocrystals were re-dispersed in hexane.

The synthesis of core-shell CdSe/nCdS nanocrystals followed the successive ion layer absorption and reaction (SILAR) approach developed by Peng and co-workers[31] with some adjustments[11]. A 250 ml r.b. flask was charged with ~2×10^{-7} moles of pre-washed CdSe cores, 5 ml of oleylamine and 5 ml of OD. Here, OD was chosen as the solvent as it alleviated the problem of precipitation observed during later stages of thick shell growth. 0.2 M elemental sulfur dissolved in OD and 0.2 M Cd-oleate in ODE were used as precursors for shell growth. The quantity of precursors for each monolayer of shell was calculated according to the volume increment of each monolayer shell, considering the changing total nanocrystal size with each successive monolayer grown. The reaction temperature was set at 240 °C. Growth times were 1 h for sulfur and 2.5 h for Cd^{2+} precursors. Reactions were continued until a desired shell thickness was achieved. The core/shell nanocrystals were washed in a similar fashion as the CdSe cores, by precipitating 2–3 times with ethanol and redispersing in hexane. Relative PL QYs were determined in comparison to a standard dye (Rhodamine 6G, 99%; Acros) and were observed to vary as a function of shell thickness. For the CdSe/9CdS nanocrystals used in the present study, the PL QY was ca. 30%. The

purified core/shell nanocrystals were studied using transmission electron microscopy (TEM) to determine their shapes and sizes and to confirm the growth of a thick CdS shell over the CdSe core.

Ligand exchange

Core/shell nanocrystals were precipitated with ethanol then centrifuged for approximately 5 min (5000 rpm). The resulting pellet was redispersed in toluene. This procedure was repeated twice. The nanocrystal concentrations were calculated according to ref. 32. An amount of ligand (mercaptoundecanoic acid) equivalent to 2 times the moles of Cd-chalcogenide in the sample was added to the toluene solution. After two hours, a solution of tetramethylammonium hydroxide in water (4 times the moles of Cd-chalcogenide) was added drop wise. The nanocrystals were transferred from the toluene phase to the water phase. The water phase was separated from the toluene phase and precipitated with isopropanol, followed by centrifugation (~5 min at 5000 rpm). Finally, the pellet was redispersed in distilled water.

Electrochemical cell

A home-built electrochemical cell with a three-electrode configuration was used. As working electrode we used an Indium Tin Oxide (ITO)-coated glass slide with sheet resistance of ~50Ω (SPI Supplies). Prior to use, the electrode was sonicated in acetone and isopropanol baths, rinsed with de-ionized water, dried and plasma-etched for 10 min. The nanocrystals were directly deposited onto the electrode from a very dilute hexane or water solution. We note that plasma etching improves significantly the attachment of water soluble nanocrystals by providing a hydrophilic surface. As a counter electrode we used platinum gauze attached to a platinum wire. The high surface area gauze was used to achieve uniform current density across the working electrode. A silver wire was used as a quasi-reference electrode. This electrode was calibrated using the $Ru^{3+/2+}$ redox-couple of $[Ru(bpy)_3](PF_6)_2$[33,34]. Based on the comparison of the half-wave potentials obtained with the silver wire, standard calomel electrode (SCE) and $Ag/Ag(NO_3)$ reference electrodes we found that the silver quasi-reference is offset from the normal hydrogen electrode (NHE) by 0.31(±0.01) V. All potentials reported in the main text are referenced to the silver quasi-reference. The electrochemical experiments were performed using several combinations of solvents (acetonitrile and propylene carbonate) and supporting electrolytes (all concentrations 0.1M): tetrabutylammonium hexafluorophosphate ($TBAPF_6$), tetrabutylammonium perchlorate ($TBAClO_4$) and lithium perchlorate ($LiClO_4$). Importantly, the results presented here are not dependent on identities of solvent, supporting electrolyte, or surface ligands.

Optical setup

The excitation source was a PicoQuant pulsed diode laser producing ~30 ps pulses at 405 nm with a repetition rate of 2.5 to 40 MHz. Most of the experiments were performed at 2.5 MHz, which corresponds to pulse-to-pulse separation of 400 ns, an order of magnitude longer than the longest PL lifetimes. This allows us to minimize “pile-up” effects and parasitic charge accumulation due to possible photocharging. The average nanocrystal excitonic occupancies generated per pulse, $\langle N \rangle$, were estimated from absorption cross-sections calculated using nanocrystal sizes derived from TEM data and were independently verified by PL saturation and intensity-dependent $g_2(0)$ measurements[35]. PL was excited and collected through an oil-immersion Olympus objective with numerical aperture NA = 1.3. After reflection from a dichroic mirror (Semrock), PL further went through a long-pass or band-pass filter (Semrock). A flip mirror was used to send emission to a 500 mm spectrometer equipped with a liquid-nitrogen-cooled silicon charge-coupled device. Emission from the nanocrystals typically peaked around 620 nm with a width of ~25 nm at

half maximum. A Hanbury-Brown-Twiss setup was realized using a 50/50 beam splitter and two avalanche photo-diodes (APDs; SPCM-AQRH-14, Perkin Elmer) with quantum efficiency ~50% at the PL wavelength, a time jitter of ~300 ps, and a dark count rate <100 Hz. The single photon counting electronics was a PicoHarp 300 stand-alone module (PicoQuant). Two APDs were used to produce start/stop signals in the measurements of the second-order intensity correlation function, whereas the synchronization pulse of the laser provided the start signal in the time-tagged time-resolved (TTTR) mode. Photon arrival times were recorded from one of the APDs (stop signal).

Analysis

For the analysis of raw TTTR data, we used the Symphotime software. All subsequent analysis and plotting were performed in Origin 8.0. For the dynamical correlated intensity – lifetime analysis, we chose a bin time, which corresponded to more than 100 photons per bin on average, to ensure a reliable bi-exponential fitting for each decay curve. We fixed the lifetimes on the basis of the values produced by the global fit procedure and constrained the amplitudes to be positive numbers. To enhance the precision, we used a Poissonian maximum likelihood estimator. To confirm the validity of the multi-exponential approach, we also constructed FLIDs for which the lifetime for each bin was calculated as a weighted average of PL photon arrival times, i.e., *without* involvement of any fitting procedure. The resulting FLIDs were similar to those produced by a multi-exponential fit, as illustrated in Supplementary Fig. 13.

Supplementary Material

Refer to Web version on PubMed Central for supplementary material.

Acknowledgments

C.G and V.I.K acknowledge support of the Center for Advanced Solar Photophysics, an Energy Frontier Research Center funded by the U.S. Department of Energy (DOE), Office of Science, Office of Basic Energy Sciences (BES). Y.G. and A.S. are supported by Los Alamos National Laboratory Directed Research and Development Fund. M.S., J.A.H, and H.H. are supported by NIH-NIGMS Grant 1R01GM084702–01. This work was conducted, in part, at the Center for Integrated Nanotechnologies, a DOE/BES user facility.

References

1. Hoogenboom JP, Hernando J, van Dijk EMHP, van Hulst NF, García-Parajó MF. Power-law blinking in the fluorescence of single organic molecules. ChemPhysChem. 2007; 8:823–833. [PubMed: 17387683]
2. Bout DAV, et al. Discrete intensity jumps and intramolecular electronic energy transfer in the spectroscopy of single conjugated polymer molecules. Science. 1997; 277:1074–1077.
3. Riley EA, Bingham C, Bott ED, Kahr B, Reid PJ. Two mechanisms for fluorescence intermittency of single violamine R molecules. Phys Chem Chem Phys. 2011; 13:1879–1887. [PubMed: 21218221]
4. Frantsuzov P, Kuno M, Janko B, Marcus RA. Universal emission intermittency in quantum dots, nanorods and nanowires. Nat Phys. 2008; 4:519–522.
5. Nirmal M, et al. Fluorescence intermittency in single cadmium selenide nanocrystals. Nature. 1996; 383:802–804.
6. Fernando D, Stefani JPH, Barkai Eli. Beyond quantum jumps: Blinking nanoscale light emitters. Physics Today. 2009; 6
7. Efros AL, Rosen M. Random telegraph signal in the photoluminescence intensity of a single quantum dot. Phys Rev Lett. 1997; 78:1110.

8. Klimov VI, Mikhailovsky AA, McBranch DW, Leatherdale CA, Bawendi MG. Quantization of multiparticle Auger rates in semiconductor quantum dots. Science. 2000; 287:1011–1013. [PubMed: 10669406]
9. Zhao J, Nair G, Fisher BR, Bawendi MG. Challenge to the charging model of semiconductor-nanocrystal fluorescence intermittency from off-state quantum yields and multiexciton blinking. Phys Rev Lett. 2010; 104:157403. [PubMed: 20482016]
10. Rosen S, Schwartz O, Oron D. Transient fluorescence of the off state in blinking CdSe/CdS/ZnS semiconductor nanocrystals is not governed by auger recombination. Phys Rev Lett. 2010; 104:157404. [PubMed: 20482017]
11. Chen Y, et al. "Giant" multishell CdSe nanocrystal quantum dots with suppressed blinking. J Am Chem Soc. 2008; 130:5026–5027. [PubMed: 18355011]
12. Mahler B, et al. Towards non-blinking colloidal quantum dots. Nat Mater. 2008; 7:659–664. [PubMed: 18568030]
13. Osovsky R, et al. Continuous-wave pumping of multiexciton bands in the photoluminescence spectrum of a single CdTe-CdSe core-shell colloidal quantum dot. Phys Rev Lett. 2009; 102:197401. [PubMed: 19518993]
14. Wang X, et al. Non-blinking semiconductor nanocrystals. Nature. 2009; 459:686–689. [PubMed: 19430463]
15. Fisher BR, Eisler HJ, Stott NE, Bawendi MG. Emission intensity dependence and single-exponential behavior in single colloidal quantum dot fluorescence lifetimes. J Phys Chem B. 2004; 108:143–148.
16. Zhang K, Chang H, Fu A, Alivisatos AP, Yang H. Continuous distribution of emission states from single CdSe/ZnS quantum dots. Nano Lett. 2006; 6:843–847. [PubMed: 16608295]
17. García-Santamaría F, et al. Breakdown of volume scaling in auger recombination in CdSe/CdS heteronanocrystals: The role of the core-shell interface. Nano Lett. 2011; 11:687–693. [PubMed: 21207930]
18. Gómez DE, van Embden J, Mulvaney P, Fernée MJ, Rubinsztein-Dunlop H. Exciton-trion transitions in single CdSe–CdS core–shell nanocrystals. ACS Nano. 2009; 3:2281–2287. [PubMed: 19655720]
19. Jha PP, Guyot-Sionnest P. Trion decay in colloidal quantum dots. ACS Nano. 2009; 3:1011–1015. [PubMed: 19341263]
20. Houtepen AJ, Vanmaekelbergh D. Orbital occupation in electron-charged CdSe quantum-dot solids. J Phys Chem B. 2005; 109:19634–19642. [PubMed: 16853539]
21. Jha PP, Guyot-Sionnest P. Electrochemical switching of the photoluminescence of single quantum dots. J Phys Chem C. 2010; 114:21138–21141.
22. Klimov VI, McGuire JA, Schaller RD, Rupasov VI. Scaling of multiexciton lifetimes in semiconductor nanocrystals. Phys Rev B. 2008; 77:195324.
23. McGuire JA, et al. Spectroscopic signatures of photocharging due to hot-carrier transfer in solutions of semiconductor nanocrystals under low-intensity ultraviolet excitation. ACS Nano. 2010; 4:6087–6097. [PubMed: 20939512]
24. Tisdale WA, et al. Hot-electron transfer from semiconductor nanocrystals. Science. 2010; 328:1543–1547. [PubMed: 20558714]
25. Li S, Steigerwald ML, Brus LE. Surface states in the photoionization of high-quality CdSe core/shell nanocrystals. ACS Nano. 2009; 3:1267–1273. [PubMed: 19374391]
26. Jeong S, et al. Effect of the thiol-thiolate equilibrium on the photophysical properties of aqueous CdSe/ZnS nanocrystal quantum dots. J Am Chem Soc. 2005; 127:10126–10127. [PubMed: 16028897]
27. Hohng S, Ha T. Near-complete suppression of quantum dot blinking in ambient conditions. J Am Chem Soc. 2004; 126:1324–1325. [PubMed: 14759174]
28. Fomenko V, Nesbitt DJ. Solution control of radiative and nonradiative lifetimes: a novel contribution to quantum dot blinking suppression. Nano Lett. 2007; 8:287–293. [PubMed: 18095736]
29. Jin S, Song N, Lian T. Suppressed blinking dynamics of single QDs on ITO. ACS Nano. 2010; 4:1545–1552. [PubMed: 20170100]

30. Tyagi P, Kambhampati P. False mulyiple exciton recombination and multiple exciton generation signals in semiconductor quantum dots arise from surface charge trapping. J Chem Phys. 2011; 134:094706. [PubMed: 21384996]

31. Li JJ, et al. Large-Scale synthesis of nearly monodisperse cdse/cds core/shell nanocrystals using air-stable reagents via successive ion layer adsorption and reaction. J Am Chem Soc. 2003; 125:12567–12575. [PubMed: 14531702]

32. Yu WW, Qu L, Guo W, Peng X. Experimental determination of the extinction coefficient of CdTe, CdSe, and CdS nanocrystals. Chem Mat. 2003; 15:2854–2860.

33. Juris A, et al. Ru(II) polypyridine complexes: photophysics, photochemistry, eletrochemistry, and chemiluminescence. Coord Chem Rev. 1988; 84:85–277.

34. DeLaive PJ, Foreman TK, Giannotti C, Whitten DG. Photoinduced electron transfer reactions of transition-metal complexes with amines. Mechanistic studies of alternate pathways to back electron transfer. J Am Chem Soc. 1980; 102:5627–5631.

35. Park YS, et al. Phys Rev Lett. 2011; 106:187401. [PubMed: 21635124]

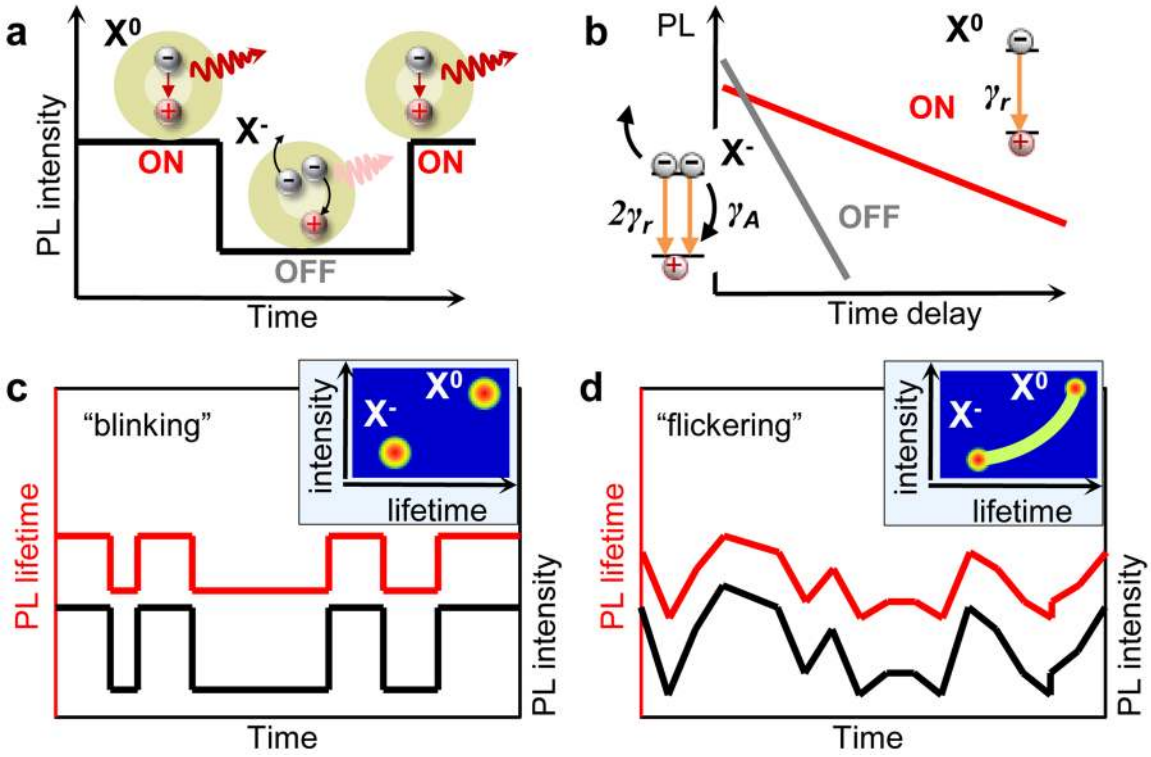

Figure 1. Conventional charging model: A-type blinking and flickering

a, In the conventional PL blinking model, ON and OFF periods correspond to a neutral (X^0) and a charged (X^-) nanocrystal, respectively. **b**, Schematic PL decay of the ON and the OFF states on a logarithmic scale. The dynamics of the ON state is dominated by the radiative rate γ_r. In the charged state, the increase in the number of recombination pathways leads to a faster radiative rate ($2\gamma_r$) responsible for the higher emission intensity at short delays. Simultaneously, the onset of three-particle Auger recombination with the rate $\gamma_A \gg \gamma_r$ opens a new nonradiative channel, leading to faster PL decay and reduced PL QY. **c**, When the time-scale of charging/discharging is longer than the experimental binning time, binary blinking is observed. **d**, For fluctuations much faster than the bin size, a continuous distribution of intensities and lifetimes is obtained, often referred to as "flickering". The insets in (**c**) and (**d**) show schematically the corresponding Fluorescence Intensity – Lifetime Distributions (FLIDs).

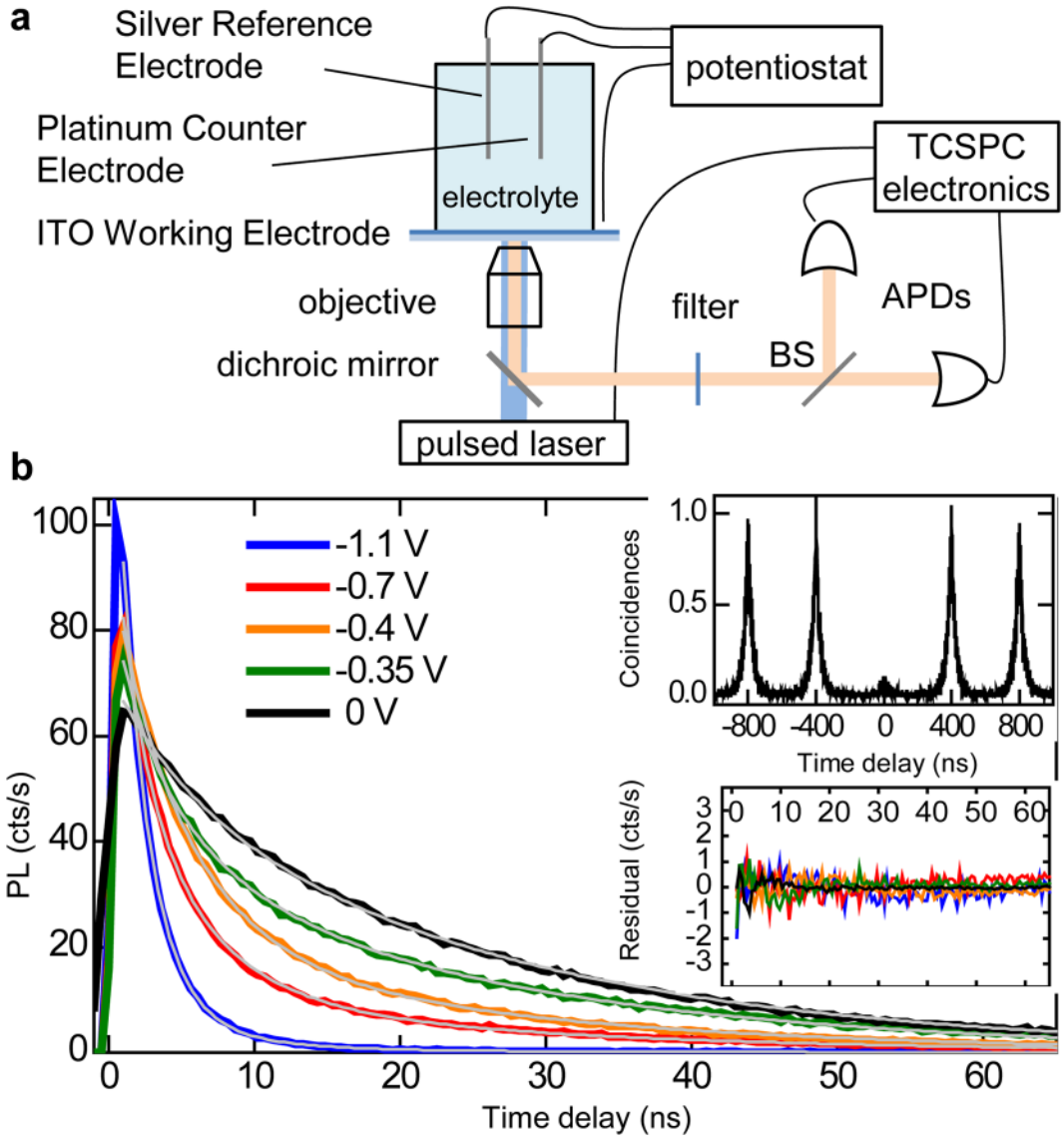

Figure 2. Experimental setup and electrochemical charging of an individual nanocrystal

a, Schematics of a single-nanocrystal spectroelectrochemical experiment. **b**, Series of PL decays for a single nanocrystal under increasing negative potential. The thin grey lines show the best global tri-exponential fit with the shared time constants, yielding the lifetimes $\tau^s = 2$ ns, $\tau^m = 5$ ns, and $\tau^l = 24$ ns. Insets: The second-order PL intensity correlation function (top) measured for this nanocrystal indicates $g_2(0) = 0.08$. Residuals of the global fit (bottom) indicate very high fidelity of the fitting procedure with deviations within the noise level and below 1% of the maximum PL signal.

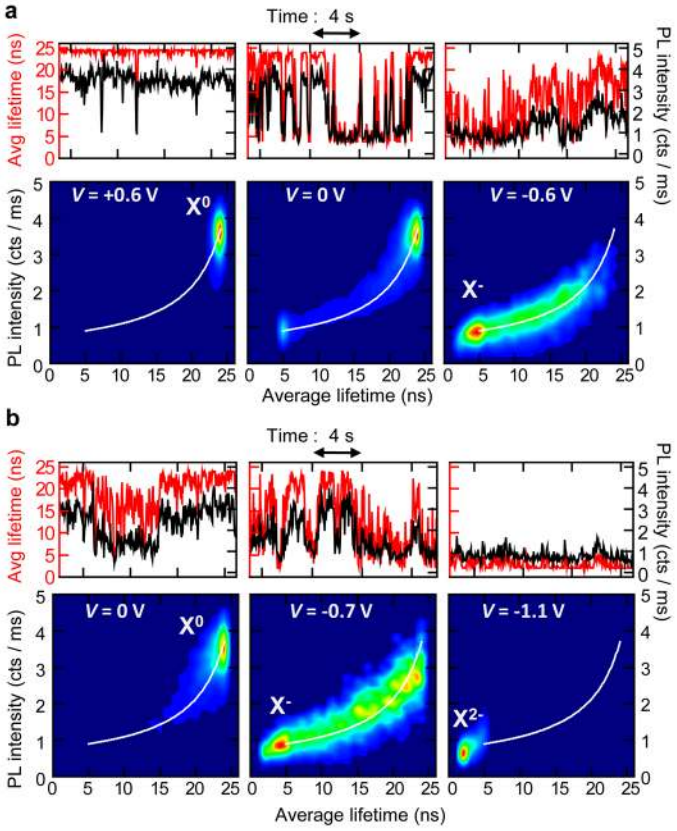

Figure 3. Correlated PL intensity and lifetime fluctuations: A-type blinking and flickering

a, PL intensity (black lines) and average lifetime (red lines) trajectories and corresponding FLIDs for the nanocrystal shown in Figs. 2b–c at three different potentials. Binary blinking seen at $V = 0$ V is suppressed at $V = +0.6$ V, whereas electron injection is achieved at $V = -0.6$ V. In the FLID color scale, red corresponds to the most frequently occurring intensity-lifetime pair, while probabilities below 1% of this maximum are represented by dark blue. A linear scaling from blue to red is used in-between. **b**, Data from the same nanocrystal, acquired on a different day, display continuous PL intensity and lifetime fluctuations, typical of flickering. At $V = -1.1$ V, we observe emission from a doubly charged exciton X^{2-}. All data were analyzed with a bin size of 50 ms. Full time trajectories for (a) and (b) are shown in Supplementary Fig. 1.

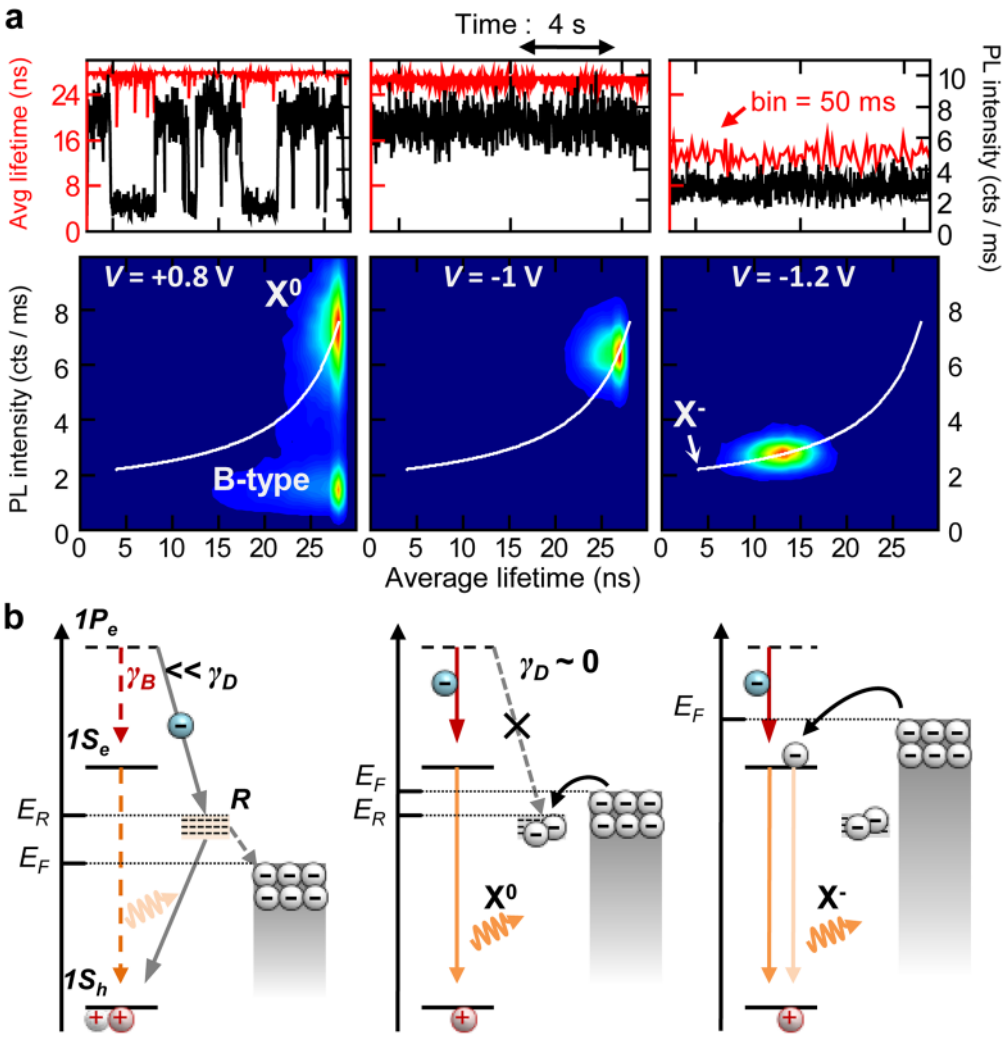

Figure 4. PL intensity fluctuations without lifetime changes: B-type blinking

a, PL intensity (black lines) and average lifetime (red lines) trajectories and corresponding FLIDs for a nanocrystal showing the B-type OFF state (labeled 'D' in FLID); analysis with a 10 ms bin. Full time trajectories are shown in Supplementary Fig. 6. **b**, The model of B-type blinking. The B-type OFF state is due to the activation of recombination centers ('*R*') that capture hot electrons with the rate γ_D which is faster than the intraband relaxation rate γ_B (the ground and the excited electron states are shown as $1S_e$ and $1P_e$, respectively). The position of the Fermi level (E_F) relative to the trap energy (E_R) is determined by the electrochemical potential and controls the occupancy of the surface trap *R*. This, in turn, allows for electrochemical control of B-type blinking.

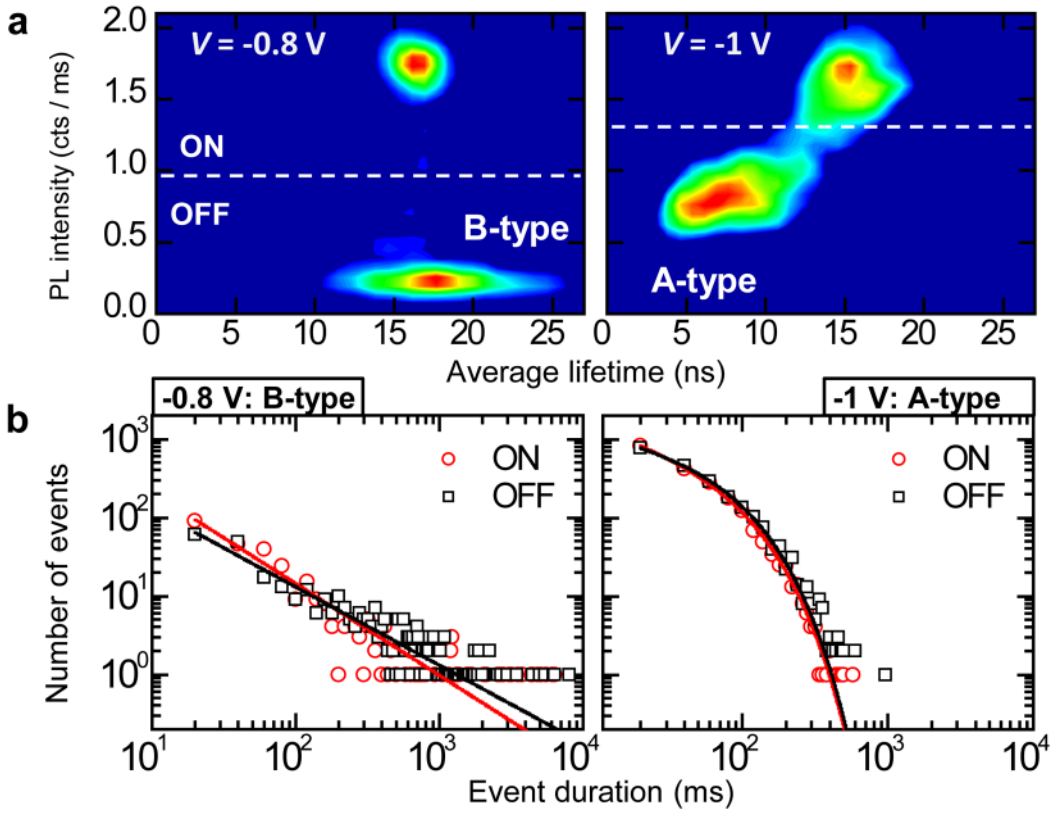

Figure 5. Electrochemically controlled switching between two distinct ON/OFF times statistics in the same nanocrystal accompanying the transition from B- to A-type blinking

a, FLIDs indicating a nanocrystal switching from B-type at −0.8 V (left) to A-type blinking at −1 V (right). Details of the analysis are given in Supplementary Fig. 9. **b,** ON (red circles) and OFF (black squares) event duration statistics for the FLIDs in '**a**' in the log-log representation. At −0.8 V, we fit the data to a power-law distribution, $\propto t^{-\alpha}$, with $\alpha = 1.17$ for the ON times (red line) and $\alpha = 1.00$ for the OFF times. At −1 V, in the A-type blinking mode, the power-law breaks down. The data, however, can be closely fitted by introducing an exponential cut-off in the form: $t^{-\alpha}\exp(-t/tc)$, where $\alpha = 0.54$, $t_c = 73.4$ ms for the ON times (red line) and $\alpha = 0.37$, $t_c = 70.8$ ms for the ON times (black line).